

Structural, electronic, and magnetic properties of 3d transition metal monatomic chains: First-principles calculations

C. Ataca,¹ S. Cahangirov,² E. Durgun,^{1,2} Y.-R. Jang,^{1,3} and S. Ciraci^{1,2,*}

¹*Department of Physics, Bilkent University, Ankara 06800, Turkey*

²*UNAM-Material Science and Nanotechnology Institute, Bilkent University, Ankara 06800, Turkey*

³*Department of Physics, University of Incheon, Incheon 402-749, Korea*

(Received 18 December 2007; revised manuscript received 8 May 2008; published 9 June 2008)

In this paper we investigated structural, electronic, and magnetic properties of 3d (light) transition metal atomic chains using first-principles pseudopotential plane-wave calculations. Infinite periodic linear, dimerized linear, and planar zigzag chain structures, as well as their short segments consisting of finite number of atoms have been considered. Like Cu, the periodic, linear chains of Mn, Co, and Ni correspond to a local shallow minimum. However, for most of the infinite periodic chains, neither linear nor dimerized linear structures are favored; to lower their energy the chains undergo a structural transformation to form planar zigzag and dimerized zigzag geometries. Dimerization in both infinite and finite chains is much stronger than the usual Peierls distortion and appears to depend on the number of 3d electrons. As a result of dimerization, a significant energy lowering occurs which, in turn, influences the stability and physical properties. Metallic linear chain of vanadium becomes half-metallic upon dimerization. Infinite linear chain of scandium also becomes half-metallic upon transformation to the zigzag structure. An interplay between the magnetic ground state and the atomic as well as the electronic structure of the chain has been revealed. The end effects influence the geometry, the energetics, and the magnetic ground state of the finite chains. Structure optimization performed using noncollinear approximation indicates significant differences from the collinear approximation. Variation of the cohesive energy of infinite- and finite-size chains with respect to the number of 3d electrons is found to mimic the well-known bulk behavior. The spin-orbit coupling of finite chains is found to be negligibly small.

DOI: [10.1103/PhysRevB.77.214413](https://doi.org/10.1103/PhysRevB.77.214413)

PACS number(s): 73.63.Nm, 75.50.Xx, 75.75.+a

I. INTRODUCTION

The fabrication of nanoscale structures, such as quantum dots, nanowires, atomic chains, and functionalized molecules, has made a great impact in various fields of science and technology.¹⁻⁴ The size and dimensionality have been shown to strongly affect the physical and chemical properties of matter.⁵ Electrons in lower dimensionality undergo a quantization which is different from that in the bulk materials.⁶⁻⁸ In nanostructures, the quantum effects, in particular the discrete nature of electronic energies with significant level spacing, become pronounced.

The suspended monatomic chains being an ultimate one-dimensional (1D) nanowire have been produced and their fundamental properties have been investigated both theoretically and experimentally.⁸⁻¹⁹ Ballistic electron transport⁶ with quantized conductance at room temperature has been observed in metallic nanowires.^{9,15} Moreover, magnetic and transport properties become strongly dependent on the details of atomic configuration. Depending on the type and position of a foreign atom or molecule that is adsorbed on a nanostructure, dramatic changes can occur in the physical properties.³ Some experimental studies, however, aimed at producing the atomic chains on a substrate.²⁰ Here the substrate-chain interaction can enter as an additional degree of freedom to influence the physical properties.

Unlike the metal and semiconductor atomic chains, not many theoretical studies are performed on transition metal²¹⁻²⁴ (TM) monatomic chains. TM monatomic chains have the ability to be magnetized much more easier the bulk.²⁵ Large exchange interactions of TM atoms in the bulk

are overcome by the large electron kinetic energies, which result in a nonmagnetic (NM) ground state with large bandwidth. On the other hand, geometries which are nonmagnetic in bulk may have magnetic ground states in monatomic chains.²⁵ In addition, it is predicted that the quantum confinement of electrons in metallic chains should result in a magnetic ground state and even in a superparamagnetic state for some of the TM chains²⁶ at finite temperatures. The central issue here is the stability of the chain and the interplay between 1D geometry and the magnetic ground state.^{21,24}

From the technological point of view, TM monatomic chains are important in the spin-dependent electronics, namely, spintronics.²⁷ While most of the conventional electronics is based on the transport of information through charges, future generation spintronic devices will take the advantage of the electron spin to double the capacity of electronics. It has been revealed that TM atomic chains either suspended or adsorbed on a 1D substrate, such as carbon nanotubes or Si nanowires, can exhibit high spin-polarity or half-metallic behavior relevant for the spin-valve effect.³ Recently, first-principles pseudopotential calculations have predicted that the finite-size segments of linear carbon chains capped by specific 3d TM atoms display an interesting even-odd disparity depending on the number of carbon atoms.²⁸ For example, CoC_nCo linear chain has an antiferromagnetic (AFM) ground state for even *n*, but the ground state changes to ferromagnetic (FM) for odd *n*. Even more interesting is the ferromagnetic excited state of an antiferromagnetic ground state can operate as a spin-valve when CoC_nCo chain is connected to metallic electrodes from both ends.²⁸

As the length of the chain decreases, finite-size effects dominate the magnetic and electronic properties.^{21,29} When

compared with the infinite case, the finite-size monatomic chains are less stable to thermal fluctuations.³⁰ Additional effects on the behavior of nanoparticle are their intrinsic properties and the interaction between them.^{29–32} The effects of noncollinear magnetism have to be taken into account as well.^{33–35} The end atoms also exhibit different behaviors with respect to the atoms close to the middle of the structure.³⁶

In this paper, we consider infinite, periodic chains of $3d$ TM atoms having linear and planar zigzag structures and their short segments consisting of finite number of atoms. For the sake of comparison, Cu and Zn chains are also included in our study. All the chain structures discussed in this paper do not correspond to the global minimum but may belong to a local minimum. The infinite and periodic geometry is of academic interest and can also be representative for very long monatomic chains. The main interest is, however, in the short segments comprising finite number of TM atoms. We examined the variation of energy as a function of the lattice constant in different magnetic states and determined stable infinite- and also finite-size chain structures. We investigated the electronic and magnetic properties of these structures. Present study revealed a number of properties of fundamental and technological interest: The linear geometry of the infinite, periodic chain is not stable for most of the $3d$ TM atoms. Even in linear geometry, atoms are dimerized to lower the energy of the chain. We found that infinite linear vanadium chains are metallic, but become half-metallic upon dimerization. The planar zigzag chains are more energetic and correspond to a local minimum. For specific TM chains, the energy can further be lowered through dimer formation within the planar zigzag geometry. Dramatic changes in the electronic properties occur as a result of dimerization. The magnetic properties of short monatomic chains have been investigated using both collinear and noncollinear approximations, which are resulted in different net magnetic moments for specific chains. Spin-orbit (SO) coupling which is calculated for different initial easy axis of magnetization has been found to be negligibly small.

II. METHODOLOGY

We have performed first-principles plane-wave calculations^{37,38} within density-functional theory³⁹ using ultrasoft pseudopotentials.⁴⁰ We also used projector augmented wave (PAW) (Ref. 41) potentials for the collinear and noncollinear spin-orbit calculations of the finite chains. The exchange-correlation potential has been approximated by generalized gradient approximation (GGA).⁴² For the partial occupancies, we have used the Methfessel–Paxton smearing method.⁴³ The widths of smearing for the infinite structures have been chosen as 0.1 eV for geometry relaxations and as 0.01 eV for the accurate energy band and the density of state calculations. As for the finite structures, the width of smearing is taken as 0.01 eV. We treated the chain structures by supercell geometry (with lattice parameters, a_{sc} , b_{sc} , and c_{sc}) using the periodic boundary conditions. A large spacing (~ 10 Å) between the adjacent chains has been assured to prevent interactions between them. In single cell calculations of the infinite systems, c_{sc} has been taken to be equal to the

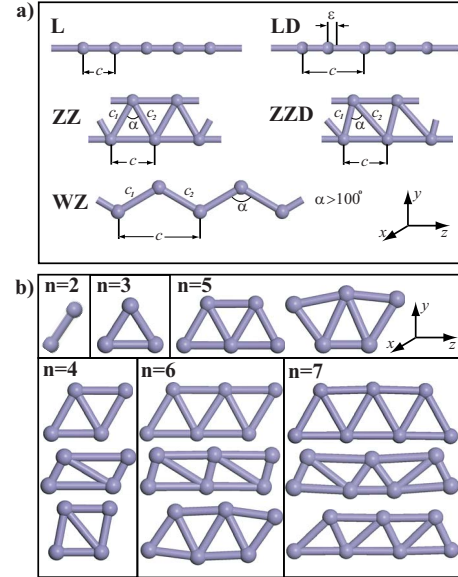


FIG. 1. (Color online) Various structures of $3d$ TM atomic chains. (a) Infinite and periodic structures; L—the infinite linear monatomic chain of TM atom with lattice constant c . LD—the dimerized linear monatomic chain with two TM atoms in the cell. ϵ is the displacement of the second atom from the middle of the unit cell. ZZ—the planar zigzag monatomic chain with lattice parameter c and unit cell having two TM atoms. $c_1 \sim c_2$ and $59^\circ < \alpha < 62^\circ$. ZZD—the dimerized zigzag structure $c_1 \neq c_2$. WZ—the wide angle zigzag structure $c_1 \sim c_2$, but with $\alpha > 100^\circ$. (b) Various chain structures of small segments consisting of finite number (n) of TM atoms, denoted by $(TM)_n$.

lattice constant of the chain. The number of plane waves used in expanding the Bloch functions and that of \mathbf{k} points used in sampling the Brillouin zone (BZ) have been determined by a series of convergence tests. Accordingly, in the self-consistent potential and the total energy calculations, the BZ has been sampled by $(1 \times 1 \times 41)$ mesh points in \mathbf{k} space within the Monkhorst–Pack scheme.⁴⁴ A plane-wave basis set with the kinetic energy cutoff $\hbar^2|\mathbf{k} + \mathbf{G}|^2/2m = 350$ eV has been used. In calculations involving PAW potentials, kinetic energy cutoff is taken as 400 eV. All the atomic positions and lattice constants (c_{sc}) have been optimized by using the conjugate gradient method where the total energy and the atomic forces are minimized. The convergence is achieved when the difference of the total energies of last two consecutive steps is less than 10^{-5} eV and the maximum force allowed on each atom is 0.05 eV/Å. As for the finite structures, supercell has been constructed in order to assure ~ 10 Å distance between the atoms of adjacent finite chain in all directions and BZ is sampled only at the Γ point. The other parameters of the calculations have been kept the same. The total energy of the optimized structure (E_T) relative to free atom energies is negative, if it is in a binding state. As a rule, the structure becomes more energetic (or stable) as its total energy is lowered. Figure 1 describes various chain structures of TM atoms treated in this study. These are the infinite periodic chains and the segments of a small number of atoms forming a string or a planar zigzag geometry. The stability of structure-optimized finite chains is further tested by displac-

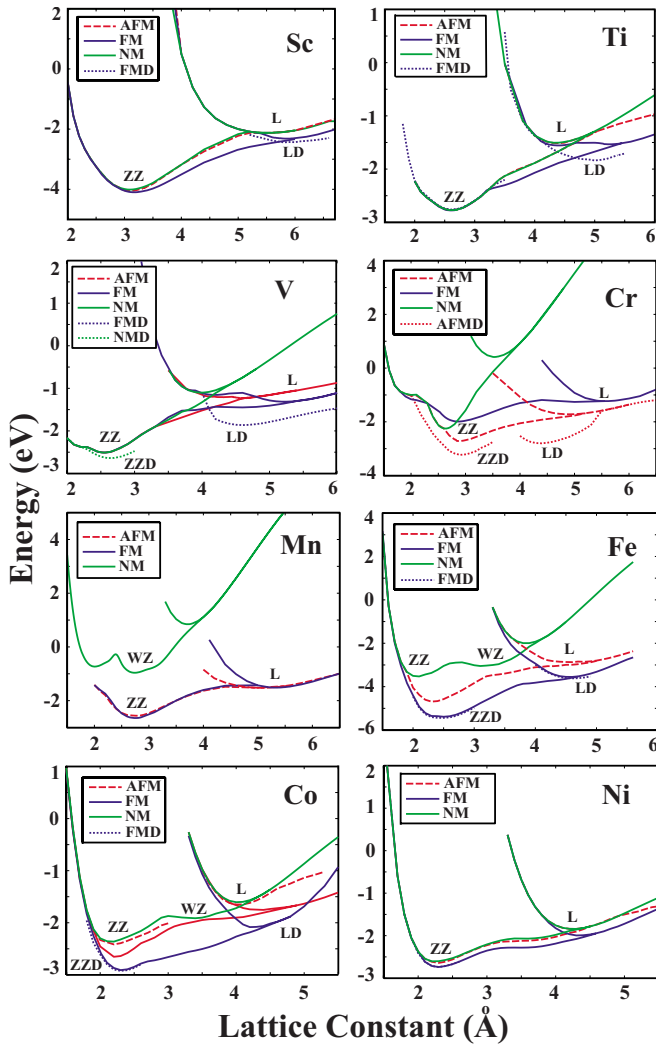


FIG. 2. (Color online) The energy versus lattice constant c of various chain structures in different magnetic states. FM—ferromagnetic, AFM—antiferromagnetic, NM—nonmagnetic, FMD—ferromagnetic state in the linear or zigzag dimerized structure, and AFMD—antiferromagnetic state in the dimerized linear or zigzag structure. The energy is taken as the energy per unit cell relative to the free constituent atom energies in their ground state (see text for definition). In order to compare the energy of the L structure with that of the LD, the unit cell (and also lattice constant) of the former is doubled in the plot. Types of structures identified as L, LD, ZZ, ZZZ, and WZ are described in Fig. 1.

ing atoms from their equilibrium positions in the plane and subsequently reoptimizing the structure. Finite-size clusters of TM atoms are beyond the scope of this paper.

III. INFINITE AND PERIODIC CHAIN STRUCTURES

Figure 2 shows the energy versus lattice constant of various infinite and periodic chain structures (described in Fig. 1) in different magnetic states. These are the infinite linear (L), the dimerized linear (LD), the planar zigzag (ZZ), and the dimerized zigzag (ZZD) monatomic chains. WZ is a

planar zigzag monatomic chain which has apical angle $\alpha > 100^\circ$. In calculating the FM state, the structure is optimized each time using a spin-polarized GGA calculations starting with a different preset magnetic moment in agreement with Hund's rule. The relaxed magnetic moment yielding to the lowest total energy has been taken as the FM state of the chain. For the AFM state, we assigned different initial spins of opposite directions to adjacent atoms and relaxed the structure. We performed spin-unpolarized GGA calculations for the NM state. The energy per unit cell relative to the free constituent atoms is calculated from the expression $E = [NE_a - E_T]$ in terms of the total energy per unit cell of the given chain structure for a given magnetic state (E_T) and the ground state energy of the free constituent TM atom E_a . N is the number of TM atom in the unit cell, which is $N=1$ for L, but $N=2$ for LD, ZZ, and ZZD structures. The minimum of E is the binding energy. By convention $E_b < 0$ corresponds to a binding structure but not necessary to a stable structure. The cohesive energy per atom is $E_c = -E_b/N$. Light transition metal atoms can have different structural and magnetic states depending on the number of their 3d electrons. For example, Sc having a single 3d electron has a shallow minimum corresponding to a dimerized linear chain structure in the FM state. If the L structure is dimerized to make a LD structure, the energy of the chain is slightly lowered. Other linear structures, such as linear NM, and AFM states have higher energy. More stable structure ZZ is, however, in the FM state. This situation is rather different for other 3d TM elements. For example, Cr has LD and more energetic ZZD structures in the AFM state. It should be noted that in the dimerized linear chain structure of Cr, the displacement of the second atom from the middle of the unit cell, ϵ , is rather large. Apparently, the dimerization is stronger than the usual Peierls distortion. As a result, the nearest neighbor distance ($c - \epsilon$) is much smaller than the second nearest neighbor distance ($c + \epsilon$). This situation poses the question whether the interaction between the adjacent dimers is strong enough to maintain the coherence of the chain structure. We address this question by comparing the energies of individual dimers

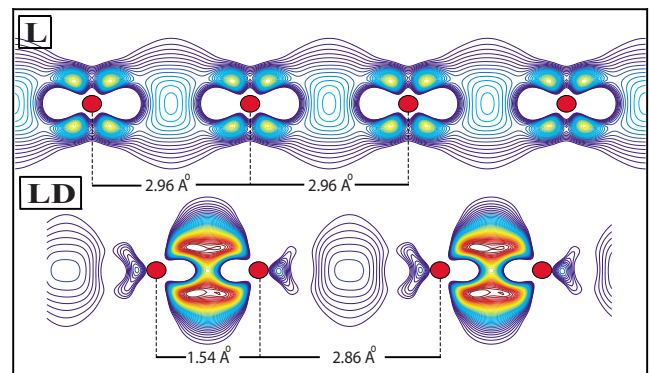


FIG. 3. (Color online) The plot of charge accumulation, namely, the positive part of the difference between the charge density of the interacting system and that of the noninteracting system for the linear (L) and the dimerized linear structure (LD) of Cr monatomic chains. The contour spacings are equal to $\Delta\rho = 0.0827 e/\text{\AA}^3$. The outermost contour corresponds to $\Delta\rho = 0.0827 e/\text{\AA}^3$. The dark balls indicate the Cr atom.

TABLE I. The calculated values for linear structures (L and LD): the lattice constant c (in Å), the displacement of the second atom in the unit cell of dimerized linear structure ϵ (in Å), the cohesive energy E_c (in eV/atom), the magnetic ground state (MGS), and the total magnetic moment μ per unit cell (in Bohr magnetons μ_B) obtained within collinear approximation.

	Sc	Ti	V	Cr	Mn	Fe	Co	Ni	Cu	Zn
c	6.0	4.9	4.5	4.4	2.6	4.6	2.1	2.2	2.3	2.6
ϵ	0.38	0.52	0.51	0.66	0.0	0.21	0.0	0.0	0.0	0.0
E_c	1.20	1.83	1.86	1.40	0.76	1.81	2.10	1.99	1.54	0.15
MGS	FM	FM	FM	AFM	AFM	FM	FM	FM	NM	NM
μ	1.74	0.45	1.00	± 1.95	± 4.40	3.32	2.18	1.14	0.0	0.0

with the chain structure. The formation of the LD structure is energetically more favorable with respect to individual dimer by 0.54 eV/atom. Furthermore, the charge accumulation, namely the positive part of the difference between the charge density of the interacting system and that of the noninteracting system, presented in Fig. 3, indicates a significant bonding between the adjacent dimers. On the other hand, the bonding in a dimer is much stronger than the one in the L chain. Nevertheless, the LD structure has to transform to more energetic ZZD structure. The zigzag structures in the AFM, FM, and NM states have minima at higher binding energies and hence are unstable.

The linear structures of Ti atoms always prefer dimerized geometries and the displacement of the second atom from the middle of the unit cell is large. There is also a remarkable energy difference between L and LD structures in favor of the latter. The energies of LD AFM, FM, and NM structures are very close to each other. Looking at the band structure of L and LD Ti chain in Fig. 7, it can easily be seen that dimerization forms flat bands which are results of localized electrons. This band structure suggests that Ti atoms form two atom molecules which interact weakly with adjacent dimer molecules. However, more energetic ZZ structures do not dimerize. All magnetic structures of V prefer to dimerize. Dimerization of V atoms also influences the magnetic and the electronic properties of the structure. One sees that the number of flat bands increases after dimerization. Vanadium is the only light TM monatomic ZZ chain which appears in

the NM lowest energy state. The linear and the linear dimerized Fe chains have a local minimum in the FM state. More stable ZZ and ZZD structures in the FM state have almost identical minima in lower binding energy. The ferromagnetic planar zigzag chain structure appears to be the lowest energy structure for Mn. Both Co and Ni monatomic chains prefer the FM state in both L and ZZ structures. The energy of ZZ chain in the FM state is lowered slightly upon dimerization. The displacement of the second atom in ZZD structure is also not very large. It is also saliency to note that Fe, Mn and Co chains in the NM state undergo a structural transformation from ZZ to WZ structure. As the number of electrons in the d shell of atom increases, the effect of dimerization on the energy and the geometry of the structure decreases. Therefore, it can be concluded that $3d$ TM atoms having fewer electrons can make hybridization easier. It is noted from Fig. 2 that the structure of $3d$ TM atomic chains is strongly dependent on their magnetic state. Optimized structural parameters, cohesive energy, magnetic state, and net magnetic moment of infinite linear and zigzag structures are presented in Tables I and II, respectively.

In Figs. 4 and 5 we compare the nearest neighbor distance and the average cohesive energy of the linear and zigzag chain structures with those of the bulk metals and plot their variations with respect to their number of $3d$ electrons of the TM atom. The nearest neighbor distance in the linear and zigzag structures is smaller than that of the corresponding bulk structure but displays similar trend. Namely, it is large for Sc having a single $3d$ electron and decreases as the num-

TABLE II. The calculated values for the planar zigzag structures (ZZ and ZZD): the lattice constant c (in Å), the first nearest neighbor c_1 (in Å), the second nearest neighbor c_2 (in Å), the angle between them α (in degrees), the cohesive energy E_c (in eV/atom), the magnetic ground state (MGS), and the total magnetic moment μ per unit cell (in Bohr magnetons μ_B) obtained within collinear approximation.

	Sc	Ti	V	Cr	Mn	Fe	Co	Ni	Cu	Zn
c	3.17	2.60	2.60	2.90	2.76	2.40	2.30	2.30	2.40	2.50
c_1	2.94	2.43	1.84	1.57	2.64	2.24	2.23	2.33	2.39	2.67
c_2	2.94	2.45	2.42	2.65	2.64	2.42	2.39	2.33	2.39	2.67
α	65.2	64.5	73.8	82.6	63.0	61.9	59.6	59.1	60.2	55.8
E_c	2.05	2.78	2.64	1.57	1.32	2.69	2.91	2.74	2.16	0.37
MGS	FM	FM	NM	AFM	FM	FM	FM	FM	NM	NM
μ	0.99	0.18	0.0	± 1.82	4.36	3.19	2.05	0.92	0.0	0.0

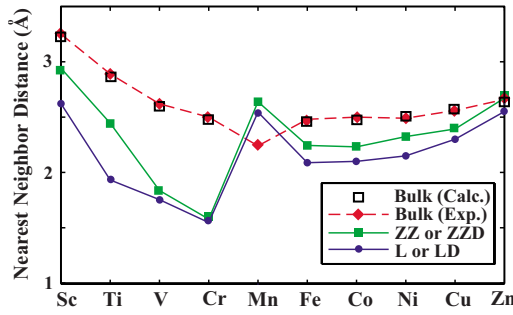


FIG. 4. (Color online) Variation of the nearest neighbor distance of 3d TM atomic chains and the bulk structures. For the linear and zigzag structures the lowest energy configuration (i.e., symmetric or dimerized one) has been taken into account. The experimental values of the bulk nearest neighbor distances have been taken from Ref. 47.

number of 3d electrons, i.e. N_d , increases to 4. Mn is an exception, since the bulk and the chain structure show opposite behavior. While the nearest neighbor distance of bulk Mn is a minimum, it attains a maximum value in the chain structure. Owing to their smaller coordination number, chain structures have smaller cohesive energy as compared to the bulk crystals as shown in Fig. 5. However, both L (or LD if it has a lower energy) and ZZ (or ZZD if it has a lower energy) also show the well-known double hump behavior which is characteristics of the bulk TM crystals. Earlier, this behavior was explained for the bulk TM crystals.^{4,45,46} The cohesive energy of zigzag structures is generally ~ 0.7 eV larger than that of the linear structures. However, it is 1–2 eV smaller than that of the bulk crystal. This implies that stable chain structures treated in this study correspond only to local minima in the Born–Oppenheimer surface.

We note that spin-polarized calculations are carried out under collinear approximation. It is observed that all chain structures presented in Tables I and II have magnetic state if $N_d < 9$. Only Cr and Mn linear chain structures and Cr zigzag

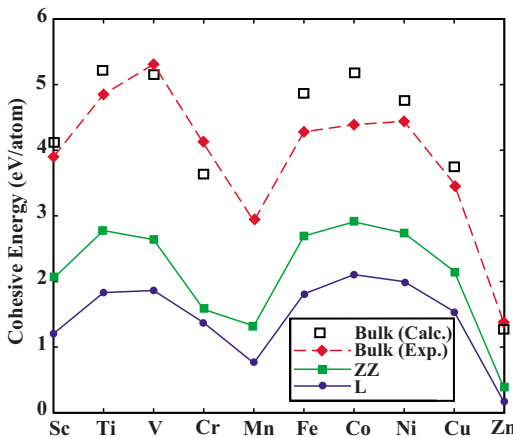


FIG. 5. (Color online) Variation of the cohesive energy E_c (per atom) of 3d TM monatomic chains in their lowest energy linear, zigzag, and bulk structures. For the linear and zigzag structures the highest cohesive energy configuration (i.e., symmetric or dimerized one) has been taken into account. The experimental values of the bulk cohesive energies have been taken from Ref. 47.

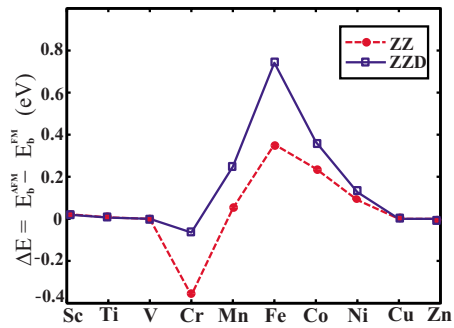


FIG. 6. (Color online) Variation of the binding energy difference ΔE (per atom) between the lowest antiferromagnetic and ferromagnetic states of 3d TM monatomic chains. The open squares and filled circles are for the symmetric zigzag ZZ and dimerized zigzag ZZD chains, respectively.

chain structure have an AFM lowest energy state. The binding energy difference between the AFM state and the FM state, $\Delta E = E_b^{\text{AFM}} - E_b^{\text{FM}}$, is calculated for all 3d TMs. Variation of ΔE with N_d is plotted in Fig. 6. We see that only Cr ZZ and ZZD chains have an AFM lowest energy state. ΔE of Fe is positive and has the largest value among all 3d TM zigzag chains. Note that ΔE increases significantly as a result of dimerization.

Having discussed the atomic structure of 3d TM chains, we next examine their electronic band structure. In Fig. 7, the chain structures in the first column do not dimerize. The linear chains placed in the third column are dimerized and changed from the L structure placed in the second column to form the LD structure. Most of the linear structures in Fig. 7 display a FM metallic character with broken spin degeneracy. A few exceptions are Mn, Cr, and V chains. The linear Mn chain has an AFM state, where spin-up (majority) and spin-down (minority) bands coincide. Chromium L and LD structures are AFM semiconductors. Vanadium is a ferromagnetic metal for both spins but becomes half-metallic upon dimerization. In half-metallic state, the chain has integer number of net spin in the unit cell. Accordingly, vanadium chain in the LD structure is metallic for one spin direction but semiconducting for the other spin direction. Hence, the spin polarization at the Fermi level, i.e. $P = [D_{\uparrow}(E_F) - D_{\downarrow}(E_F)] / [D_{\uparrow}(E_F) + D_{\downarrow}(E_F)]$, is 100%. Bands of Cu and Zn with filled 3d shell in nonmagnetic state are in agreement with previous calculations.⁴⁸ In Fig. 8, the chain structures in the first column have only ZZ structure. The zigzag chains in the second column are transformed to a lower energy (i.e. more energetic) ZZD structure in the third column. The ZZ chain of Sc is stable in a local minimum and displays a half-metallic character with 100% spin-polarization at the Fermi level. Accordingly, a long segment of ZZ chain of Sc can be used as a spin valve. Ti, Mn, and Ni in their stable zigzag structures are FM metals. The stable ZZD structures of Fe and Co chains are also FM metals. The ZZ and relatively lower energy ZZD structure of V chain are nonmagnetic. Both ZZ and ZZD structures of Cr are in the AFM state.

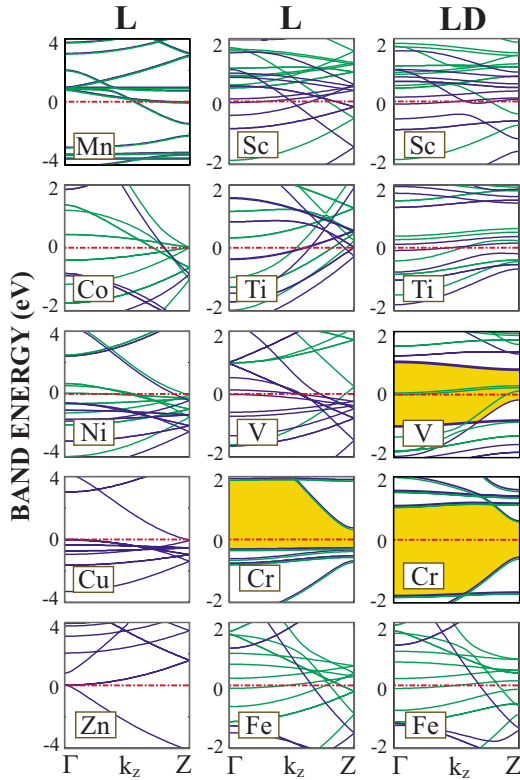


FIG. 7. (Color online) Energy band structures of 3d TM atomic chains in their L and LD structures. The zero of energy is set at the Fermi level. The gray and black lines are the minority and majority bands, respectively. In the antiferromagnetic state majority and minority bands coincide. The energy gaps between the valence and the conduction bands are shaded.

For Co and Fe in the ZZD structure more bands of one type of spin cross the Fermi level as compared to those of the other type of spin resulting in a high spin polarization at the Fermi level. This situation implies that in the ballistic electron transport, the conductance of electrons with one type of spin is superior to electrons with the opposite type of spin, namely, $\sigma_{\downarrow} \gg \sigma_{\uparrow}$. Accordingly, the conductance of electrons across Fe and Co chains becomes strongly dependent on their spin directions. This behavior of the infinite periodic Fe or Co chain is expected to be unaltered to some extent for long but finite chains and can be utilized as a spin-dependent electronic device. In closing this section, we want to emphasize that the infinite, periodic chains of 3d TM atoms can be in the zigzag structure corresponding to a local minimum. However, most of the zigzag structures are dimerized. Dimerization causes remarkable changes in electronic and magnetic properties.

IV. SHORT CHAIN STRUCTURES

Periodic infinite chains in Sec. III are only ideal structures; long finite-size segments perhaps can attain their physical properties revealed above. On the other hand, the end effects can be crucial for short segments consisting of few atoms which may be important for various spintronic applications. In this section, we examine short segments of 3d TM chains consisting of n atoms, where $n=2-7$.

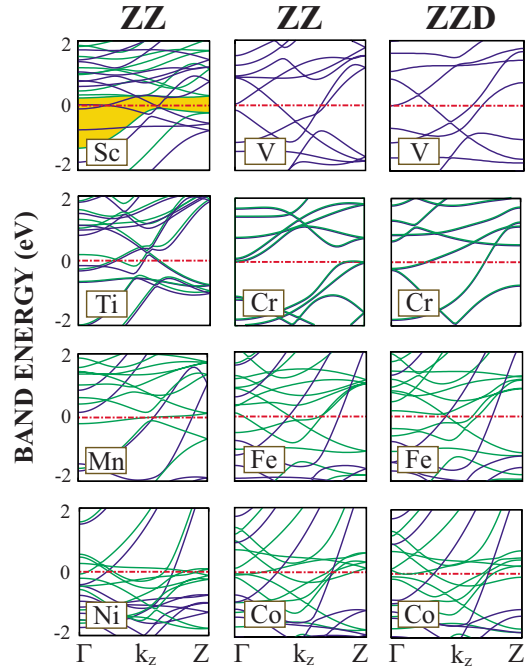


FIG. 8. (Color online) Energy band structures of 3d TM atomic chains in their ZZ and ZZD structures. The zero of energy is set at the Fermi level. The gray and black lines are minority and majority spin bands, respectively. The gray and dark lines coincide in the antiferromagnetic state. Only the dark lines describe the bands of nonmagnetic state. The energy gap between the valence and the conduction bands is shaded.

A. Collinear approximation

We first study the atomic structure and magnetic properties of the finite chains within collinear approximation using ultrasoft pseudopotentials.⁴⁰ The linear structure is unstable for the finite-size segments. Various planar zigzag structures, which are only local minima, are described in Fig. 1. We optimized the geometry of these zigzag structures with different initial conditions of magnetic moment on the atoms within collinear approximation. If the final optimized structures for q different initial conditions result in different average cohesive energy (or different total energy), they may actually be trapped in different local minima. Here we considered the following different initial conditions: (1) At the beginning, opposite magnetic moments $\pm\mu_a$ have been assigned to adjacent atoms, and the total magnetic moment, $\mu = \sum\mu_a$, has been forced to vanish at the end of optimization for $n=2-7$. Initial magnetic moment μ_a on atoms is determined from the Hund rule. (2) For $n=2-7$, initial magnetic moments of all atoms have been taken in the same direction, but the final magnetic moment of the structure has been determined after optimization without any constraint. (3) For $n=2-7$, the system is relaxed using spin-unpolarized GGA. (4) For $n=2-7$, initial magnetic moments of chain atoms have been assigned as is done in (1), but $\mu = \sum\mu_a$ is not forced to vanish in the course of relaxation. (5) For $n=2-7$, spin-polarized GGA calculations have been carried out without assigning any initial magnetic moment. (6) We have assigned the magnetic moments $\uparrow\downarrow\downarrow\uparrow$ for $n=4$ and $\uparrow\downarrow\downarrow\downarrow\uparrow$ for

TABLE III. The average cohesive energy E_c (in eV/atom), the net magnetic moment μ (in Bohr magneton μ_B), the magnetic ordering (MO), and the LUMO-HOMO gap of majority and/or minority states, E_G^\uparrow and E_G^\downarrow , respectively (in eV) for lowest energy zigzag structures. p/q indicates that the same optimized structure occurred p times starting from q different initial conditions (see text). Results have been obtained by carrying out structure optimization within collinear approximation using the ultrasoft pseudopotentials.

	ZZ	Sc	Ti	V	Cr	Mn	Fe	Co	Ni	Cu	Zn
$n=2$	E_c	0.83	1.38	1.29	0.93	0.32	1.29	1.49	1.38	1.14	0.02
	μ	4.0	2.0	2.0	0.0	10.0	6.0	4.0	2.0	0.0	0.0
	$E_G^\uparrow/E_G^\downarrow$	0.59/1.60	0.29/1.01	1.03/1.22	2.17/2.17	2.04/0	1.14/0.59	1.42/0.36	1.48/0.27	1.59/1.59	3.96/3.96
	MO	FM	FM	FM	AFM	FM	FM	FM	FM	NM	NM
	$p(q=5)$	2	1	2	1	1	2	2	1	3	3
$n=3$	E_c	1.30	1.87	1.61	0.91	0.63	1.72	1.84	1.78	1.24	0.12
	μ	1.0	6.0	3.0	6.0	15.0	10.0	7.0	2.0	1.0	0.0
	$E_G^\uparrow/E_G^\downarrow$	0.66/0.44	0.45/1.08	0.31/0.78	1.23/2.03	1.66/0.35	0.39/0.58	0.19/0.18	0.87/0.24	0.08/1.55	2.96/2.96
	MO	FM	NM								
	$p(q=5)$	3	1	2	2	1	2	3	3	1	3
$n=4$	E_c	1.54	2.13	2.01	1.16	0.84	2.07	2.31	2.08	1.61	0.13
	μ	4.0	2.0	2.0	0.0	18.0	14.0	10.0	4.0	0.0	0.0
	$E_G^\uparrow/E_G^\downarrow$	0.37/0.36	0.46/0.50	0.35/0.30	1.16/0.61	1.16/0.50	1.47/0.04	1.98/0.34	1.10/0.25	0.96/0.96	2.35/2.35
	MO	FM	FM	FM	AFM*	FM	FM	FM	FM	NM	NM
	$p(q=6)$	5	3	4	4	4	2	1	3	3	3
$n=5$	E_c	1.63	2.27	2.08	0.83	0.91	2.25	2.46	2.23	1.74	0.15
	μ	3.0	0.0	0.0	0.0	5.0	16.0	11.0	6.0	1.0	0.0
	$E_G^\uparrow/E_G^\downarrow$	0.29/0.46	0.43/0.43	0.49/0.40	0.47/0.52	1.12/0.30	1.42/0.56	1.53/0.37	1.47/0.09	1.42/0.90	1.96/1.96
	MO	FM	AFM*	AFM*	AFM*	FM	FM	FM	FM	FM	NM
	$p(q=6)$	3	4	2	4	4	1	1	3	1	3
$n=6$	E_c	1.69	2.32	2.26	1.29	1.02	2.31	2.50	2.29	1.75	0.17
	μ	8.0	0.0	0.0	0.0	0.0	20.0	14.0	6.0	2.0	0.0
	$E_G^\uparrow/E_G^\downarrow$	0.22/0.29	0.44/0.44	0.54/0.54	0.53/0.55	0.41/0.38	1.33/0.41	0.30/0.32	0.28/0.10	1.42/0.95	1.88/1.88
	MO	FM	AFM	AFM	AFM*	AFM*	FM	FM	FM	FM	NM
	$p(q=7)$	3	3	7	4	4	2	4	4	1	3
$n=7$	E_c	1.74	2.38	2.22	1.25	1.06	2.35	2.58	2.36	1.84	0.18
	μ	7.0	6.0	5.0	6.0	5.0	22.0	15.0	8.0	1.0	0.0
	$E_G^\uparrow/E_G^\downarrow$	0.01/0.33	0.34/0.21	0.32/0.48	0.54/0.68	0.85/0.42	0.95/0.29	0.98/0.17	0.83/0.09	0.79/0.61	1.77/1.77
	MO	FM	NM								
	$p(q=7)$	5	3	6	4	5	1	2	4	1	3

$n=5$. Here different spacings between two spin arrows indicate different bond lengths. This way different exchange couplings for different bond lengths and hence dimerization is accounted. (7) The initial magnetic moments on atoms $\uparrow\downarrow\downarrow\uparrow$ for $n=6$ and $\uparrow\downarrow\uparrow\uparrow\downarrow\downarrow\uparrow$ for $n=7$ have been assigned. (8) Similar to (7), initial magnetic moments $\uparrow\downarrow\uparrow\downarrow\downarrow\uparrow$ and $\uparrow\downarrow\downarrow\uparrow\downarrow\uparrow$ have been assigned for $n=6$ and $n=7$, respectively. Last three initial conditions are taken into consideration due to the fact that different bond lengths of $3d$ TM atoms affect the type of magnetic coupling between consecutive atoms.²⁴ The initial atomic structures have been optimized for these initial conditions except Cu and Zn. Only first three conditions are consistent with Cu and Zn. As the initial geometry, a segment of n atoms has been extracted from the optimized infinite zigzag chain and placed in a supercell, where the

interatomic distance between adjacent chains was greater than 10 \AA for all atoms. Our results are summarized in Table III, where the magnetic orders having the same lowest total energy occurred p times from q different initial conditions are presented. In this respect the magnetic ordering in Table III may be a potential candidate for the magnetic ground state.

The average cohesive energy of finite-size chains increases with increasing n . In Fig. 9, we plot the average cohesive energy of these small segments consisting of n atoms. For the sake of comparison, we presented the plots for the linear and zigzag structures. The average values of cohesive energy in Fig. 9(b) are taken from Table III. We note three important conclusions drawn from these plots. (i) The cohesive energies of the zigzag structures are consistently

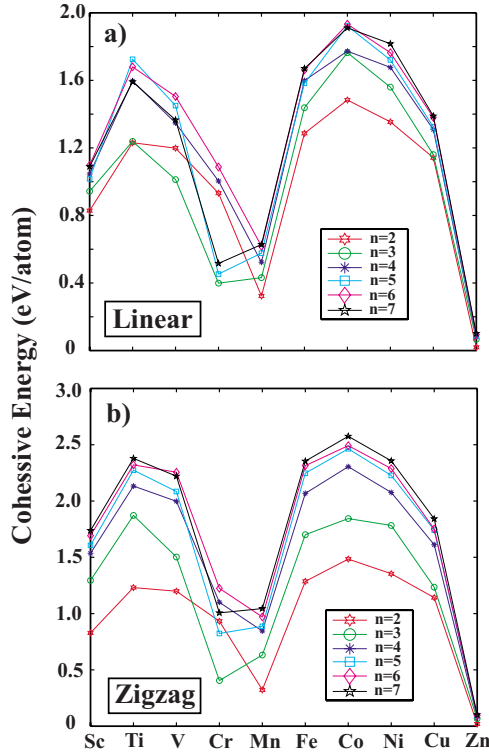


FIG. 9. (Color online) Variation of the average cohesive energy of small segments of chains consisting of n atoms. (a) The linear chains; (b) the zigzag chains. In the plot, the lowest energy configurations for each case obtained by optimization from different initial conditions.

larger than those of the linear structures, and the cohesive energies also increase with increasing n . (ii) For each types of structures, as well as for each n , the variation of E_c with respect to the number of $3d$ electrons in the outer shell, N_d , exhibits a double hump shape, which is typical of the bulk and the infinite chain structures as presented in Fig. 5. (iii) For specific cases $E_c(n_2) < E_c(n_1)$, even if $n_2 > n_1$ (V and Cr). This situation occurs because the total energy cannot be lowered in the absence of dimerization.

Most of the finite zigzag chain structure of $3d$ TM atoms has a FM lowest energy state. The magnetic ordering specified by AFM* for specific chains indicates that the magnetic moment on individual atoms, μ_a , may be in opposite directions or may have unequal magnitudes, but the total magnetic moment, $\mu = \sum \mu_a$, adds up to zero. The finite chains of Zn atoms are always nonmagnetic for all n . Finite zigzag chains of Cu are nonmagnetic for even n , except $n=6$. Interestingly, the dimerized linear chain of Cr ($n=5$) with a FM lowest energy state is more energetic than that of the zigzag chain given in Table III. The geometry of this structure is such that two dimers consisting of two atoms are formed at both ends of the linear structure and a single atom at the middle is located equidistant from both dimers. The distance from the middle atom to any of the dimers is approximately twice the distance between the atoms in the dimer. Even though the nearest neighbor distance of the middle atom to dimers is long, there is a bonding between them. The cohesive energy is ~ 0.2 eV higher than that of the zigzag case,

and the total magnetic moment of the structure ($6\mu_B$) is provided by the atom at the middle. This is due to the fact that two dimers at both ends are coupled in the AFM order. This is an expected result because the cohesive energy (per atom) of Cr₂ is higher than that of Cr₅ in the zigzag structure. The lowest unoccupied molecular orbital (LUMO)/highest occupied molecular orbital (HOMO) gap for majority and minority spin states usually decreases with increasing n . However, depending on the type of TM atom, the maximum value of the gap occurs for different number n of atoms. The zigzag chains of Zn atoms usually have the largest gap for a given n .

Even though the total magnetic moment, $\mu = \sum \mu_a$, of the AFM* state vanishes for the finite molecule, LUMO-HOMO gaps for majority and minority states are not generally the same as in the AFM state. This can be explained by examining the magnetic moment on every individual atom and the geometry of the molecule. For Cr₄, the magnetic moment on each atom is lined up as described in the sixth initial condition. In this ordering, two dimers each consisting of two atoms are in the AFM ordering within themselves, but in the FM ordering with each other. The distribution of final magnetic moment on atoms for Mn₆ also obeys one of the initial conditions [case (7)]. Three dimers each consisting of two atoms coupled in the AFM order within themselves, but in the FM order with each other. Similar results are also obtained for other AFM* states.

The zigzag planar structure for $n > 3$ in Table III corresponds to a local minimum. To see whether the planar zigzag structures are stable or else it transforms to other geometry by itself is a critical issue. To assure that the finite chain structures of $n=4$ and $n=7$ in Table III are stable in a local minimum, we first displaced the atoms out of planes, then we optimized the structure. Upon relaxation all displaced atoms returned to their equilibrium position on the plane.

B. Noncollinear approximation and the spin-orbit interaction

In cases where both AFM and FM couplings occur and compete with each other, collinear magnetism fails for modeling the ground state magnetic ordering. A midway between AFM and FM exchange interactions results in allowing the spin quantization axis to vary in every site of the structure. Geometric structure also influences noncollinear magnetism. Frustrated antiferromagnets having triangular lattice structure, disordered systems, as well as broken symmetry on the surface will result in noncollinear magnetism. Spin glasses, α -Mn, domain walls, and Fe clusters are typical examples of noncollinearity. Finite structures that are studied in this paper all have low symmetry and AFM-FM coupling competition, which increase the probability of observing noncollinear magnetism. Coupling the magnetic moment to the crystal structure (spin-orbit coupling) plays an important role in determining the direction of easy axes of magnetization. This magnetization axis influences magnetic anisotropy and it is required for determining the magnetic behavior of the structure in a magnetic field. Due to the geometry of the finite molecules studied in this paper, shape and magnetocrystalline anisotropy are expected to result in noncollinear magnetism. For further information on noncollinear magnetism, see Refs. 49–54.

The finite chains discussed in Sec. III within collinear approximation will now be treated using noncollinear approximation. To this end, the structure of chains has been optimized starting from the same initial geometry [starting from a segment of n atoms extracted from the optimized infinite ZZ (or ZZD) chain placed in a supercell] and five different initial configurations of spins on individual atoms. (i) The direction of the initial magnetic moment on the atoms is consecutively altered as $xyzy$. (ii) No preset directions are assigned to the individual atoms; they are determined in the course of structure optimization using noncollinear approximation. (iii) For each triangle, the initial magnetic moment on the atoms has a nonzero component only in the xy plane, but $(\sum_{\Delta} \mu_a)_{xy} = 0$. (Here “ Δ ” stands for the summation over the atoms forming a triangle.) (iv) Similar to (iii), but $(\sum_{\Delta} \mu_a)_z \neq 0$. (v) In a zigzag chain, the magnetic moments of atoms on the lower row are directed along the z axis, while those on the upper row are directed in the opposite direction. Using these five different initial conditions on the magnetic moment of individual atoms, the initial atomic structure is optimized using both ultrasoft⁴⁰ pseudopotentials and PAW (Ref. 41) potentials. We first discuss the results obtained by using ultrasoft pseudopotentials. Almost all of the total magnetic moment and the cohesive energy of the optimized structures have been in good agreement with those given in Table III (obtained within collinear approximation). However, there are some slight changes for specific finite structures. For example, Sc_7 is found to have magnetic moment of $7\mu_B$ in collinear approximation. Even though one of the initial conditions in noncollinear calculations resulted in the same magnetic moment and energy, we also found a state which has 0.01 eV lower total energy with the total magnetic moment of $9\mu_B$. The same situation also occurred with PAW potential. Ti_5 has a special magnetic moment distribution which is the same for both ultrasoft and PAW cases and will be explained below. In collinear approximation, V_5 is noted to have zero magnetic moment; nevertheless, there is a state of 0.03 eV lower in energy which is FM with $\mu=1$. Even though Co_7 has the same total magnetic moment in both collinear and noncollinear cases, there is a significant energy difference between two cases.

Noncollinear calculations have also been performed using PAW potentials (which is necessary for the spin-orbit coupling calculations) starting with five different initial assignments of magnetic moments as described above. Most of our calculations have yielded the same magnetic moment distribution with previous calculations, but there are still few cases which are resulted differently. Mn_7 is an exception; all structure optimization starting from different initial conditions resulted in a nonplanar geometry. Note that in collinear and noncollinear calculations using ultrasoft pseudopotential Mn_7 was stable in a local minimum corresponding to the planar zigzag geometry, but it formed a cluster when spin-orbit coupling and noncollinear effects are taken into account by using PAW potentials. Unlike other $n=5$ zigzag structures, Ti_5 has a unique ordering of the atomic magnetic moments. Two Ti atoms on the upper row have magnetic

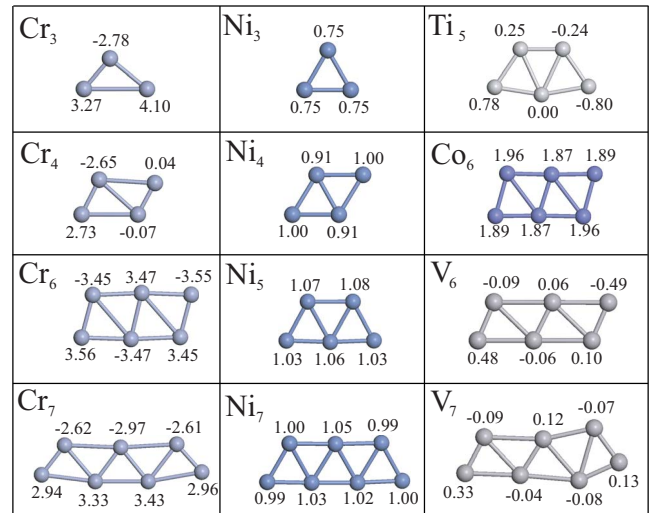


FIG. 10. (Color online) The atomic magnetic moments of some finite chains of $3d$ transition metal atoms. Numerals on the atomic sites stand for the value of the atomic magnetic moments. Positive and negative numerals are for spin-up and spin-down polarizations, respectively. Because of finite-size of the zigzag chains, the end effects are usually appear by different values of magnetic moments on atoms at the end of the chain.

moments which are in opposite directions. Similarly, two Ti atoms at the ends of the lower row also have atomic magnetic moments in opposite directions, but the magnitudes of moments are smaller than those of on the upper row. The atom at the middle of the lower row has no magnetic moment. In $n=6$ case, only Co_6 has a nonvanishing magnetic moment. Other atoms form dimers which are coupled in the AFM order. If we assume that the shape of $n=6$ molecule is parallelogram, there is an AFM coupling between the atoms on both diagonals. In addition to these, remaining two atoms in the middle also coupled in the AFM order, as indicated in Fig. 10. Cr_n chains exhibit an even-odd disparity; Cr_n has an AFM ordering for even n , but it has a FM ordering for odd n . There are also cases where collinear and noncollinear calculations with ultrasoft pseudopotential resulted in an excited state for the magnetic moment distribution. Although PAW potential calculations found the same magnetic ordering with collinear and ultrasoft noncollinear cases, there are even more energetic states for Sc_6 , V_4 , Cr_5 as shown in Fig. 11, and Mn_5 given in Table IV. Geometric dimerization also plays an important role in determining the average cohesive energy. Due to the magnetic ordering and the dimerization of atoms in the finite molecules, the average cohesive energy may not always increase as the number of atoms in the molecule increases. V_6 and V_7 , Cr_6 and Cr_7 , Ni_5 and Ni_6 are examples where magnetization and dimerization effects are most pronounced. It should be denoted that Hobbs *et al.*⁴⁹ carried out noncollinear calculations with the PAW potential on Cr_{2-5} and Fe_{2-5} finite chain structures. Here, our results on Cr_{2-5} are in agreement with those of Hobbs *et al.*⁴⁹

Among several $3d$ -atomic chains, Ni_6 and Mn_6 are only chains for which noncollinear effects are most pronounced as shown in Fig. 11. For the other structures, noncollinear magnetic moments on the atoms deviate slightly from the collinear case.

TABLE IV. The highest average cohesive energy E_c (in eV/atom), the components (μ_x, μ_y, μ_z) and the magnitude of the net magnetic moment μ (in μ_B), the LUMO-HOMO gap E_G (SO coupling excluded) or energy gap after spin-orbit coupling was included in the x direction or in the z direction (in eV), the magnetic ordering (MO), the spin-orbit coupling energy $\Delta E_{SO}^x / \Delta E_{SO}^z$ (in meV) under the x and z initial directions of easy axes of magnetization. $p(q=5)$ indicates that the same optimized structure occurred p times starting from q ($=5$) different initial conditions. Results have been obtained by carrying out structure optimization calculations within noncollinear approximation using PAW potentials. Mn_7 is not stable in the planar ZZ structure. For the (x, y, z) directions, see Fig. 1(b). These values belong to the most energetic configuration determined by noncollinear calculations including spin-orbit coupling.

	ZZ	Sc	Ti	V	Cr	Mn	Co	Ni
$n=2$	E_c	0.85	1.56	1.58	0.53	0.47	1.50	1.60
	$(\mu_x, \mu_y, \mu_z), \mu$	(2.3, 2.3, 2.3), 4.0	(0.0, 0.0, 2.0), 2.0	(1.2, 1.1, 1.2), 2.0	(0.0, 0.0, 0.0), 0.0	(1.1, -0.2, 9.9), 10.0	(2.8, 2.9, 0.0), 4.0	(1.7, 1.0, 0.0), 2.0
	$E_G / E_G^x / E_G^z$	0.49/0.18/0.17	0.36/0.36/0.36	0.67/0.67/0.66	0.56/1.87/1.87	0.18/0.18/0.18	0.05/0.05/0.05	0.18/0.17/0.30
	MO	FM	FM	FM	AFM	FM	FM	FM
	$\Delta E_{SO}^x / \Delta E_{SO}^z$	3.60/3.80	4.70/3.90	8.30/8.00	10.90/10.90	13.30/13.50	0.01/9.90	33.30/32.50
	$p(q=5)$	4	4	5	3	3	5	4
$n=3$	E_c	1.36	2.00	1.91	0.72	0.70	1.90	2.04
	$(\mu_x, \mu_y, \mu_z), \mu$	(0.4, 0.9, -0.1), 1.0	(2.2, 2.3, 2.4), 4.0	(0.6, 0.6, 0.6), 1.0	(5.6, 2.2, 0.0), 6.0	(1.4, -2.7, 0.1), 3.0	(0.3, 0.6, 7.0), 7.0	(0.7, 1.4, 1.3), 2.0
	$E_G / E_G^x / E_G^z$	0.37/0.37/0.37	0.26/0.26/0.25	0.44/0.44/0.44	1.01/1.01/1.01	0.25/0.24/0.24	0.34/0.11/0.12	0.11/0.11/0.10
	MO	FM	FM	FM	FM	FM	FM	FM
	$\Delta E_{SO}^x / \Delta E_{SO}^z$	3.70/3.70	4.70/4.70	8.40/8.40	10.40/10.50	13.10/13.00	8.20/9.60	33.10/32.70
	$p(q=5)$	4	2	3	2	1	1	5
$n=4$	E_c	1.60	2.36	2.35	0.89	1.02	2.29	2.33
	$(\mu_x, \mu_y, \mu_z), \mu$	(0.6, 1.7, 0.9), 2.0	(1.1, 1.2, 1.2), 2.0	(0.0, 0.0, 0.0), 0.0	(0.0, 0.0, 0.0), 0.0	(0.0, 0.0, 0.0), 0.0	(4.6, 4.6, 4.7), 8.0	(-0.8, -2.1, 3.3), 4.0
	$E_G / E_G^x / E_G^z$	0.29/0.29/0.29	0.41/0.41/0.41	0.28/0.28/0.28	1.09/1.09/1.09	0.30/0.30/0.30	0.03/0.03/0.03	0.06/0.21/0.20
	MO	FM	FM	AFM	AFM	AFM	FM	FM
	$\Delta E_{SO}^x / \Delta E_{SO}^z$	3.70/3.70	4.70/4.70	8.40/8.40	10.30/10.20	13.20/13.20	8.30/8.80	32.10/ 32.20
	$p(q=5)$	3	4	2	1	3	5	2
$n=5$	E_c	1.67	2.49	2.46	1.00	1.22	2.50	2.46
	$(\mu_x, \mu_y, \mu_z), \mu$	(0.8, 0.1, 0.6), 1.0	(0.0, 0.0, 0.0), 0.0	(0.7, 0.5, 0.6), 1.0	(2.5, 2.5, 1.9), 4.0	(-1.3, 1.7, -2.1), 3.0	(-2.4, 10.6, -1.4), 11.0	(2.4, 5.5, -0.1), 6.0
	$E_G / E_G^x / E_G^z$	0.26/0.26/0.26	0.34/0.34/0.34	0.27/0.27/0.27	0.28/0.44/0.44	0.09/0.21/0.21	0.33/0.33/0.33	0.14/0.01/0.01
	MO	FM	AFM	FM	FM	FM	FM	FM
	$\Delta E_{SO}^x / \Delta E_{SO}^z$	3.80/3.50	4.80/4.80	8.20/8.20	10.40/10.40	14.10/13.00	8.90/8.90	33.90/ 34.20
	$p(q=5)$	4	4	3	1	1	2	5
$n=6$	E_c	1.75	2.53	2.57	1.26	1.31	2.56	2.49
	$(\mu_x, \mu_y, \mu_z), \mu$	(0.0, 0.0, 0.0), 0.0	(0.0, 0.0, 0.0), 0.0	(0.0, 0.0, 0.0), 0.0	(0.0, 0.0, 0.0), 0.0	(0.0, 0.0, 0.0), 0.0	(6.7, 6.7, 7.3), 12.0	(0.0, 0.0, 0.0), 0.0
	$E_G / E_G^x / E_G^z$	0.19/0.19/0.19	0.32/0.32/0.32	0.38/0.38/0.38	0.77/0.77/0.77	0.48/0.48/0.48	0.20/0.20/0.20	0.20/0.17/0.17
	MO	AFM	AFM	AFM	AFM	AFM	FM	AFM
	$\Delta E_{SO}^x / \Delta E_{SO}^z$	3.70/3.70	4.70/4.70	8.10/8.10	10.30/10.30	13.20/13.30	8.00/8.40	32.30/32.30
	$p(q=5)$	1	4	5	1	4	5	5
$n=7$	E_c	1.82	2.60	2.57	1.14		2.65	2.60
	$(\mu_x, \mu_y, \mu_z), \mu$	(5.2, 5.2, 5.2), 9.0	(1.1, 2.8, 0.0), 3.0	(0.1, 1.0, 0.0), 1.0	(-0.2, -0.2, 6.0), 6.0		(8.6, 8.7, 8.7), 15.0	(-2.6, 7.5, 0.3), 8.0
	$E_G / E_G^x / E_G^z$	0.15/0.15/0.15	0.19/0.19/0.20	0.24/0.24/0.24	0.39/0.39/0.39		0.09/0.09/0.09	0.09/0.05/0.05
	MO	FM	FM	FM	FM		FM	FM
	$\Delta E_{SO}^x / \Delta E_{SO}^z$	3.80/3.80	4.90/4.80	8.20/8.20	10.60/10.40		8.30/8.50	33.70/33.50
	$p(q=5)$	2	1	5	2		5	5

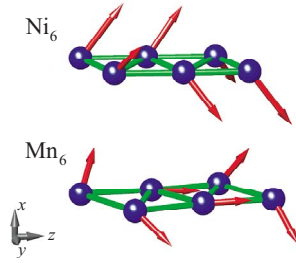


FIG. 11. (Color online) Atomic magnetic moments of Ni_6 and Mn_6 planar zigzag chains calculated by noncollinear approximation including spin-orbit interaction. The magnitudes and directions of magnetic moments are described by the length and direction of arrows at each atom.

We calculated the effects of spin orbit coupling (SO) energy as well. In making fully self-consistent calculations, we first assumed that initial easy axis of magnetization of the structure is along x or z direction. As shown in Fig. 1(b), x direction is perpendicular to the plane of atoms and z direction is the axis along the chain. This way, spinor wave functions are let rotate from their initial orientation until the magnetic moment is parallel to the easy axis of magnetization which is determined in the course of structure optimization. Here, the optimized structure of every initial condition together with the calculated magnetic moment on the individual atoms are used for the calculation of SO coupling. The optimized structures of $(\text{TM})_n$ and atomic magnetic moments have been determined within noncollinear approximation using PAW potentials. Spin-orbit coupling energy is defined by the expansion, $\Delta E_{\text{SO}}^{x/z} = (E_T^{x/z} - E_T^0)/n$, where $E_T^{x/z}$ and E_T^0 are the total energies of the chain calculated within noncollinear approximation with and without spin-orbit interaction in the x/z direction, respectively. The highest average cohesive energy E_c given in Table IV is obtained using the expression $E_c = (nE_a - E_T^{x/z})/n$, where E_a is the ground state energy of the free constituent TM atom. $E_T^{x/z}$ is the lowest value of E_T^x and E_T^z . As can be easily seen SO coupling does not play an important role on the energy of the planar finite structure. However, SO coupling becomes crucial when the total magnetic moments, which happen to be oriented in different directions owing to the different initial conditions, result in the same energy. It is easily observed that in most of the structures both initial directions of easy axis of magnetization resulted in the same SO coupling energy. This means that it is the most probable that fully self-consistent structure optimization of SO coupling calculations resulted in the lowest energy easy axis of magnetization. For this reason other initial directions of easy axis of magnetization were not calculated. In addition, ΔE_{SO}^x and ΔE_{SO}^z appear to be independent of n except Mn_5 , Co_2 and Co_3 . It is also observed that when SO coupling is taken into account, LUMO-HOMO gap energies decrease. Only for Ni_4 , Cr_5 , Mn_5 and Ni_7 , LUMO-HOMO gap increased due to the fact that the final geometry of SO coupling calculations has further relaxed slightly from that of noncollinear calculations.

V. CONCLUSION

In this paper, we presented an extensive study of the structural, electronic and magnetic properties of monatomic chains of $3d$ transition metal atoms (Sc, Ti, V, Cr, Mn, Fe, Co, Ni, as well as Cu and Zn) using first-principles plane-wave methods. We considered infinite and periodic chains (with linear, dimerized linear, zigzag, and dimerized zigzag geometries) and small finite-size chains including two to seven atoms. Due to the end effects, we found differences between infinite chains and finite ones. Therefore, we believe that the basic understanding of monatomic TM chains has to comprise both infinite and finite structures as done in the present paper.

The infinite, dimerized linear structures have a shallow minimum only for a few TM atoms; planar zigzag and dimerized zigzag structures, however, correspond to a lower binding energy providing stability in this geometry. As for short chains consisting of four to seven TM atoms, the planar zigzag structure is only a local minimum. The finite chains tend to form clusters if they overcome energy barriers. We found close correlation between the magnetic state and the geometry of the chain structure. In this study, we presented the variation of binding energy as a function of the lattice constant for different structures and the magnetic states. We also revealed the dependence of the electronic and magnetic properties on the atomic structures of the chains. We found that the geometric structure influences strongly the electronic and magnetic properties of the chains. For example, infinite linear V chain becomes half-metallic upon dimerization. Similarly, infinite dimerized linear and metallic Sc chain becomes half-metallic with 100% spin polarization at the Fermi level upon transformation to zigzag structure. Furthermore, while the infinite linear Mn chain has an antiferromagnetic ground state, with $\mu = \sum \mu_a = 0$, but $|\sum \mu_a^1| = |\sum \mu_a^2| = 4.40 \mu_B$, it becomes a ferromagnetic metal with $\mu = \sum \mu_a = 4.36 \mu_B$ as a result of the structural transformation from linear to dimerized zigzag structure.

Magnetic ordering of finite-size chains becomes more complex and requires a treatment using noncollinear approximation. The structure optimizations carried out using ultrasoft pseudopotentials generally result in the same cohesive energy and magnetic moment in both collinear and noncollinear approximations. However, for specific finite chains the total magnetic moments calculated by using PAW potentials with the same initial magnetic moment distribution differ dramatically from ultrasoft results. Of course, our results which cover much more than 3000 different structure optimizations may not include the lowest energy state but indicate the importance of noncollinear treatment.

ACKNOWLEDGMENTS

Part of the computational resources for this study has been provided through Grant No. 2-024-2007 by the National Center for High Performance Computing of Turkey, Istanbul Technical University.

*ciraci@fen.bilkent.edu.tr

- ¹K. Tsukagoshi, B. W. Alphenaar, and H. Ago, *Nature* (London) **401**, 572 (1999).
- ²S. Ciraci, A. Buldum, and I. P. Batra, *J. Phys.: Condens. Matter* **13**, R537 (2001).
- ³S. Ciraci, S. Dag, T. Yildirim, and O. Gulseren, *J. Phys.: Condens. Matter* **16**, R901 (2004); E. Durgun, D. Cakir, N. Akman, and S. Ciraci, *Phys. Rev. Lett.* **99**, 256806 (2007).
- ⁴Y. Mokrousov, G. Bihlmayer, S. Blügel, and S. Heinze, *Phys. Rev. B* **75**, 104413 (2007).
- ⁵C. M. Schneider and J. Kirschner, in *Handbook of Surface Science*, edited by K. Horn and M. Scheffler (Elsevier, Amsterdam, 2000), pp. 511–668.
- ⁶B. J. van Wees, H. van Houten, C. W. J. Beenakker, J. G. Williamson, L. P. Kouwenhoven, D. van der Marel, and C. T. Foxon, *Phys. Rev. Lett.* **60**, 848 (1988).
- ⁷P. Gambardella, A. Dallmeyer, K. Maiti, M. C. Malagoli, W. Eberhardt, K. Kern, and C. Carbone, *Nature* (London) **416**, 301 (2002).
- ⁸N. Agrait, A. L. Yeyati, and J. M. van Ruitenbeek, *Phys. Rep.* **377**, 81 (2003).
- ⁹A. I. Yanson, G. Rubio-Bollinger, H. E. van den Brom, N. Agrait, and J. M. van Ruitenbeek, *Nature* (London) **395**, 783 (1998).
- ¹⁰H. Ohnishi, Y. Kondo, and K. Takayanagi, *Nature* (London) **395**, 780 (1998).
- ¹¹M. R. Sorensen, M. Brandbyge, and K. W. Jacobsen, *Phys. Rev. B* **57**, 3283 (1998).
- ¹²H. Hakkinen, R. N. Barnett, and U. Landman, *J. Phys. Chem. B* **103**, 8814 (1999).
- ¹³D. Sánchez-Portal, E. Artacho, J. Junquera, P. Ordejón, A. Garcia, and J. M. Soler, *Phys. Rev. Lett.* **83**, 3884 (1999).
- ¹⁴J. A. Torres, E. Tosatti, A. D. Corso, F. Ercolessi, J. J. Kohanoff, F. D. Di Tolla, and J. M. Soler, *Surf. Sci.* **426**, L441 (1999).
- ¹⁵M. Okamoto and K. Takayanagi, *Phys. Rev. B* **60**, 7808 (1999).
- ¹⁶V. Rodrigues, T. Fuhrer, and D. Ugarte, *Phys. Rev. Lett.* **85**, 4124 (2000).
- ¹⁷P. Sen, S. Ciraci, A. Buldum, and I. P. Batra, *Phys. Rev. B* **64**, 195420 (2001).
- ¹⁸P. Sen, O. Gulseren, T. Yildirim, I. P. Batra, and S. Ciraci, *Phys. Rev. B* **65**, 235433 (2002).
- ¹⁹S. Tongay, R. T. Senger, S. Dag, and S. Ciraci, *Phys. Rev. Lett.* **93**, 136404 (2004).
- ²⁰O. Gurlu, H. J. W. Zandvliet, B. Poelsema, S. Dag, and S. Ciraci, *Phys. Rev. B* **70**, 085312 (2004).
- ²¹J. Dorantes-Davila and G. M. Pastor, *Phys. Rev. Lett.* **81**, 208 (1998).
- ²²A. Delin and E. Tosatti, *J. Phys.: Condens. Matter* **16**, 8061 (2004).
- ²³A. Bala, T. Nautiyal, and K. S. Kim, *Phys. Rev. B* **74**, 174429 (2006).
- ²⁴Y. Mokrousov, G. Bihlmayer, S. Heinze, and S. Blügel, *Phys. Rev. Lett.* **96**, 147201 (2006).
- ²⁵A. Delin and E. Tosatti, *Phys. Rev. B* **68**, 144434 (2003).
- ²⁶M. Wierzbowska, A. Delin, and E. Tosatti, *Phys. Rev. B* **72**, 035439 (2005).
- ²⁷S. A. Wolf, D. D. Awschalom, R. A. Buhrman, J. M. Daughton, S. von Molnár, M. L. Roukes, A. Y. Chtchelkanova, and D. M. Treger, *Science* **294**, 1488 (2001).
- ²⁸E. Durgun, R. T. Senger, H. Mehrez, H. Sevincli, and S. Ciraci, *J. Chem. Phys.* **125**, 121102 (2006).
- ²⁹R. H. Kodama, *J. Magn. Magn. Mater.* **200**, 359 (1999).
- ³⁰H. Kachkachi, *J. Magn. Magn. Mater.* **316**, 248 (2007).
- ³¹V. L. Moruzzi, *Phys. Rev. Lett.* **57**, 2211 (1986).
- ³²M. Luban, *J. Magn. Magn. Mater.* **272-276**, e635 (2004).
- ³³V. Heine, J. H. Samson, and C. M. M. Nex, *J. Phys. F: Met. Phys.* **11**, 2645 (1981).
- ³⁴P. Gambardella, *J. Phys.: Condens. Matter* **15**, S2533 (2003).
- ³⁵M. B. Knickelbein, *Phys. Rev. B* **70**, 014424 (2004).
- ³⁶R. F. Wallis, *Phys. Rev.* **105**, 540 (1957).
- ³⁷M. C. Payne, M. P. Teter, D. C. Allen, T. A. Arias, and J. D. Joannopoulos, *Rev. Mod. Phys.* **64**, 1045 (1992).
- ³⁸Numerical computations have been carried out by using VASP software, G. Kresse and J. Hafner, *Phys. Rev. B* **47**, 558 (1993); G. Kresse and J. Furthmüller, *ibid.* **54**, 11169 (1996).
- ³⁹W. Kohn and L. J. Sham, *Phys. Rev.* **140**, A1133 (1965); P. Hohenberg and W. Kohn, *Phys. Rev.* **136**, B864 (1964).
- ⁴⁰D. Vanderbilt, *Phys. Rev. B* **41**, 7892 (1990).
- ⁴¹G. Kresse and D. Joubert, *Phys. Rev. B* **59**, 1758 (1999).
- ⁴²J. P. Perdew, J. A. Chevary, S. H. Vosko, K. A. Jackson, M. R. Pederson, D. J. Singh, and C. Fiolhais, *Phys. Rev. B* **46**, 6671 (1992).
- ⁴³M. Methfessel and A. T. Paxton, *Phys. Rev. B* **40**, 3616 (1989).
- ⁴⁴H. J. Monkhorst and J. D. Pack, *Phys. Rev. B* **13**, 5188 (1976).
- ⁴⁵A. Sommerfeld and H. Bethe, *Handbuch der Physik* (Springer, Berlin, 1933).
- ⁴⁶J. Friedel, in *The Physics of Metals*, edited by J. M. Ziman (Cambridge University Press, New York, 1969); D. G. Pettifor, in *Solid State Physics*, edited by H. Ehrenreich and D. Turnbull (Academic, New York, 1987), Vol. 40, p. 43.
- ⁴⁷C. Kittel, *Introduction to Solid State Physics*, 7th ed. (Wiley, New York, 1996).
- ⁴⁸J. C. Tung and G. Y. Guo, *Phys. Rev. B* **76**, 094413 (2007).
- ⁴⁹D. Hobbs, G. Kresse, and J. Hafner, *Phys. Rev. B* **62**, 11556 (2000).
- ⁵⁰Ph. Kurz, F. Förster, L. Nordström, G. Bihlmayer, and S. Blügel, *Phys. Rev. B* **69**, 024415 (2004).
- ⁵¹J. Anton, B. Fricke, and E. Engel, *Phys. Rev. A* **69**, 012505 (2004).
- ⁵²J. Kübler, K.-H. Höck, J. Sticht, and A. R. Williams, *J. Phys. F: Met. Phys.* **18**, 469 (1988).
- ⁵³T. Oda, A. Pasquarello, and R. Car, *Phys. Rev. Lett.* **80**, 3622 (1998).
- ⁵⁴S. Sharma, J. K. Dewhurst, C. Ambrosch-Draxl, S. Kurth, N. Helbig, S. Pittalis, S. Shallcross, L. Nordström, and E. K. U. Gross, *Phys. Rev. Lett.* **98**, 196405 (2007).